

THE LICK-INDEX CALIBRATION OF THE GEMINI MULTI-OBJECT SPECTROGRAPHS

THOMAS H. PUZIA

Department of Astronomy and Astrophysics, Pontificia Universidad Católica de Chile, Avenida Vicuña Mackenna 4860, Macul, Santiago, Chile, *tpuzia@astro.puc.cl*

BRYAN W. MILLER AND GELYS TRANCHO¹

Gemini Observatory, Casilla 603, La Serena, Chile, *bmiller@gemini.edu*

BRETT BASARAB²

Middlebury College, Middlebury, VT 05753, USA

JORDAN T. MIROCHA²

Center for Astrophysics and Space Astronomy, University of Colorado, 389 UCB, Boulder, CO 80309, USA

AND

KAREN BUTLER³

National Optical Astronomy Observatory, 950 N. Cherry Ave., Tucson, AZ 85719, USA

To appear in The Astronomical Journal

ABSTRACT

We present the calibration of the spectroscopic Lick/IDS standard line-index system for measurements obtained with the Gemini Multi-Object Spectrographs known as GMOS-North and GMOS-South. We provide linear correction functions for each of the 25 standard Lick line indices for the B600 grism and two instrumental setups, one with 0.5'' slit width and 1×1 CCD pixel binning (corresponding to ~ 2.5 Å spectral resolution) and the other with 0.75'' slit width and 2×2 binning (~ 4 Å). We find small and well-defined correction terms for the set of Balmer indices $H\beta$, $H\gamma_A$, and $H\delta_A$ along with the metallicity sensitive indices Fe5015, Fe5270, Fe5335, Fe5406, Mg₂ and Mg*b* that are widely used for stellar population diagnostics of distant stellar systems. We find other indices that sample molecular absorption bands, such as TiO₁ and TiO₂, with very wide wavelength coverage or indices that sample very weak molecular and atomic absorption features, such as Mg₁, as well as indices with particularly narrow passband definitions, such as Fe4384, Ca4455, Fe4531, Ca4227, and Fe5782, less robustly calibrated. These indices should be used with caution.

Subject headings: Methods: data analysis, Techniques: spectroscopic

1. INTRODUCTION

The spectroscopic Lick index system was introduced by Burstein et al. (1984) in order to homogenize the study of low-resolution integrated-light spectra of elliptical galaxies and other extragalactic stellar systems. It is based on observations carried out with the Cassegrain image dissector scanner (IDS) spectrograph at the 3-m Shane telescope of the Lick Observatory and has been continuously updated and refined by several subsequent works (e.g. Worthey et al. 1994; Worthey & Ottaviani 1997; Trager et al. 1998). In its current form it defines 25 widely-used line indices for specific atomic and molecular absorption features in the optical wavelength range from ~ 4040 to ~ 6420 Å. The precise definition of line index passbands allows a reproducible measurement and uniform interpretation of spectroscopic data, in particular of index combinations sensitive to luminosity-weighted stellar population age and various chemical abundances. Because the Lick system was initially devised to study

the integrated-light spectra of massive early-type galaxies with high velocity dispersions (Burstein et al. 1984; Worthey 1994; Worthey & Ottaviani 1997), the spectral indices are defined for low spectral resolution at about $R \lesssim 700$ which is equivalent to a spectral resolution of 8–11 Å in the optical, (see Fig. 7 in Worthey & Ottaviani 1997). However, higher resolution index definitions which are formally more sensitive to the absorption feature of interest (e.g. Vazdekis et al. 2010) deliver lower signal-to-noise with the same instrumental setup and exposure time. In general, spectral resolution and integration times have to be traded for any index system to yield the most efficient observing program and most robust index measurements depending on the target luminosity.

That said, the great advantage of the Lick system is its comprehensive library of nearby-star stellar spectra covering a large parameter space in $\log g$, T_{eff} , and metallicity. This library is the foundation of many population synthesis models that use fitting functions computed from this library (Tripicco & Bell 1995) to model predictions of Lick index strengths as a function stellar-population age and chemical composition for simple and composite stellar populations (see e.g. Trager et al. 2000; Thomas et al. 2003, 2004). One can then use

¹ G.T.'s present address: GMTO Corporation, P.O. Box 90933, Pasadena, CA 91109

² AURA/CTIO Research Experience for Undergraduates (REU) participant

³ 2004 Gemini South internship, University of Victoria

such model predictions to derive ages and chemical makeups of distant stellar populations, such as galaxies (e.g. Thomas et al. 2005) and globular clusters (e.g. Puzia et al. 2005), provided the observed spectra match the spectroscopic characteristics of the IDS Lick spectrograph in terms of wavelength coverage, spectroscopic resolution, and continuum flux calibration. Calibrating spectroscopic index measurements onto the Lick system is usually done by re-observing stars from the Lick standard star library (Worthey et al. 1994) with the same instrumental configuration that is being used for science observations (see e.g. Puzia et al. 2002). The purpose of this work is to provide such Lick index calibrations for the Gemini Multi-Object Spectrographs at the Gemini North and Gemini South Observatory for the most commonly used B600 grating and spectrograph setups.

2. OBSERVATIONS

All spectroscopic observations were collected using both telescopes of the Gemini Observatory. The first campaign was conducted with the Gemini Multi-Object Spectrograph (GMOS) on the 8.2-m Gemini-North telescope on Mauna Kea in Hawaii (hereafter GMOS-N) as part of the programs GN-2002A-Q-17, GN-2002B-Q-77, GN-2003A-Q-75, and GN-2004A-Q-94. The second campaign took place at the 8.2-m Gemini-South telescope on Cerro Pachón in Chile (hereafter GMOS-S) as part of programs GS-2003B-Q-63 and GS-2004A-Q-62 (see Table 1 for a log of all GMOS observations).

2.1. Sample Selection

The stars observed by us are so-called ‘secondary Lick standards’ that were used to derive the fitting functions in many population synthesis models (Worthey 1994; Faber et al. 1985; Trager et al. 1998). Since most of these sample stars were observed only 1-3 times at Lick observatory (except for HD184406 and HD165760 which were observed 64 and 40 times, respectively) part of the scatter in the calibrations will be associated with the uncertainties in the Lick measurements themselves. Our star sample is a subset of the total Lick/IDS standard star list selected by H. Kuntschner for the SAURON integral field spectrograph project (Kuntschner et al. 2006). The selection criteria are: 1) $-10^\circ < \text{Dec} < 70^\circ$; 2) the star must be part of the Henry Draper (HD) Catalogue (see Nesterov et al. 1995, and references therein); and 3) the star must not be classified as peculiar. There are 233 stars in this subset spread across all R.A. coordinates. The SAURON project observed 73 of these stars as part of its survey of the dynamics and stellar populations of nearby early-type galaxies. Our sub-sample summarized in Table 1 facilitates therefore a comparison and cross-calibration option between SAURON and GMOS, and previous results from other instruments.

2.2. Spectrograph Configuration

At the time of our observations the twin GMOS instruments provided a wavelength coverage within 3600–9400 Å in long-slit and multi-slit mode over a $5.5' \times 5.5'$ field of view. The instruments are equipped with three EEV CCDs with $2.8''$ gaps between the detector chips. Since the gaps run perpendicular to the dispersion direction, we took dithered sub-integrations with two different grating blaze angles (at $\lambda = 508$ and 510 nm) to cover the

entire wavelength range. All standard star observations were performed in long-slit mode with the B600 grating with a wavelength coverage from 3800–6500 Å with a resolution of $R \approx 1500$. The ‘‘central spectrum’’ region of interest on the CCD detector was used to place the standard star along the spatial axis of the slit and to reduce the size of the corresponding files.

For the GMOS-N observations we used two instrumental setups with different detector chip binning factors and slit widths. In the following we refer to setting A as the configuration with 2×2 detector binning and $0.75''$ slit width (6 stars with 13 individual observations) and to setting B with 1×1 binning and $0.5''$ slit width (11 stars with 35 individual observations). Most of the GMOS-N observations were conducted using the standard procedure of centering the target in the slit, however for GN-2003A-Q-75 the observations were unguided and the telescope was nodded such that the light from the stars moved across the narrow dimension of the slit aperture (perpendicular to the spatial axis and parallel to the dispersion axis). With this technique the light from the star fills the slit and the spectral resolution depends only on the slit width. The detectors were the original E2V devices EEV9273-16-03, EEV9273-20-04, and EEV9273-20-03. All observations at GMOS-S were conducted with the B setting (14 stars with 28 individual exposures). The detectors were E2V devices EEV 2037-06-03, EEV 8194-19-04, and EEV 8261-07-04. All the GMOS-S observations were carried out with the nodding method described above.

3. DATA REDUCTION

The data were reduced using common procedures for long-slit data. The Gemini GMOS IRAF package was used for most reduction steps. These scripts are mostly wrappers for standard IRAF⁴ tasks that handle the Gemini Multi-Extension FITS (MEF) data format. Differences from standard Gemini procedures are noted below.

3.1. Bias Subtraction and Flat Fielding

Bias subtraction was performed using average bias frames (0 second exposure time) taken the closest in time to a given Lick dataset. It proved best to subtract the overscan from the average biases and the science data as the bias level drifts slowly with time. Care must be taken to use only the area of overscan that is farthest from the detector area so that the overscan is free from any contamination. This helps reducing artificial ‘‘jumps’’ in the spectra due to bias subtraction.

Flat field frames were created from quartz halogen lamp spectra taken before or after the Lick star exposures. The quartz lamp signature was removed using a wrapper script for the IRAF RESPONSE task. Since the effective slit length was shortened by using the ‘‘central spectrum’’ region of interest, twilight flats were not used to apply an illumination correction.

3.2. Wavelength Calibration

⁴ IRAF is distributed by the National Optical Astronomy Observatories, which are operated by the Association of Universities for Research in Astronomy, Inc., under cooperative agreement with the National Science Foundation.

TABLE 1
JOURNAL OF GMOS-N AND GMOS-S OBSERVATIONS

Star	Program	Observing Date	Slit width	Binning	Grating	Blaze λ [nm]	t_{exp} [sec]
HD074377	GN-2002A-Q-17	2002-02-12	0.75''	2 × 2	B600_G5303	508,510	120,60
HD148816	GN-2002A-Q-17	2002-02-15	0.75''	2 × 2	B600_G5303	508,510	5,5
HD165195	GN-2002A-Q-17	2002-03-09	0.75''	2 × 2	B600_G5303	508,510	20,20
HD172401	GN-2002A-Q-17	2002-03-09	0.75''	2 × 2	B600_G5303	508,510	20,20
HD172958	GN-2002A-Q-17	2002-03-14	0.75''	2 × 2	B600_G5303	508,510	20,20
HD199580	GN-2002A-Q-17	2002-04-17	0.75''	2 × 2	B600_G5303	508,510,510	10,10,5
<hr/>							
HD224930	GN-2002B-Q-77	2002-10-08	0.5''	1 × 1	B600_G5303	2x(508,512)	4x30
HD017709	GN-2002B-Q-77	2002-10-08	0.5''	1 × 1	B600_G5303	508,512	45,45
HD034411	GN-2002B-Q-77	2002-10-08	0.5''	1 × 1	B600_G5303	508	4
HD224930	GN-2002B-Q-77	2002-10-09	0.5''	1 × 1	B600_G5303	508,512,4x508	30,30,120,3x300
HD019373	GN-2002B-Q-77	2002-10-09	0.5''	1 × 1	B600_G5303	508,512,512	120,60,120
HD020893	GN-2002B-Q-77	2002-10-09	0.5''	1 × 1	B600_G5303	508	120
HD097907	GN-2003A-Q-75	2003-04-28	0.5''	1 × 1	B600_G5303	508,512	180,300
HD143761	GN-2003A-Q-75	2003-04-28	0.5''	1 × 1	B600_G5303	508,512	180,180
HD147677	GN-2003A-Q-75	2003-04-28	0.5''	1 × 1	B600_G5303	508,512	300,300
HD172401	GN-2003A-Q-75	2003-06-02	0.5''	1 × 1	B600_G5303	508,512	120,120
HD161817	GN-2004A-Q-94	2004-06-15	0.5''	1 × 1	B600_G5303	2x(508,512)	4x60
HD168720	GN-2004A-Q-94	2004-06-15	0.5''	1 × 1	B600_G5303	508,512	60,60
<hr/>							
HD200779	GS-2003B-Q-63	2003-09-27	0.5''	1 × 1	B600_G5323	508,512	60.5,60.5
HD207076	GS-2003B-Q-63	2003-09-27	0.5''	1 × 1	B600_G5323	508,512	90.5,90.5
HD219617	GS-2003B-Q-63	2003-09-27	0.5''	1 × 1	B600_G5323	508,512	90.5,90.5
HD175638	GS-2003B-Q-63	2003-10-01	0.5''	1 × 1	B600_G5323	508,512	60.5,60.5
HD184406	GS-2003B-Q-63	2003-10-01	0.5''	1 × 1	B600_G5323	508,512	60.5,60.5
HD184492	GS-2003B-Q-63	2003-10-01	0.5''	1 × 1	B600_G5323	508,512	60.5,60.5
HD036003	GS-2003B-Q-63	2003-10-02	0.5''	1 × 1	B600_G5323	508,512	60.5,60.5
HD064606	GS-2003B-Q-63	2003-11-01	0.5''	1 × 1	B600_G5323	508,512	60.5,60.5
HD043318	GS-2003B-Q-63	2003-11-02	0.5''	1 × 1	B600_G5323	508,512	60.5,60.5
HD037160	GS-2003B-Q-63	2003-11-02	0.5''	1 × 1	B600_G5323	508,512	60.5,60.5
HD049161	GS-2003B-Q-63	2003-11-02	0.5''	1 × 1	B600_G5323	508,512	60.5,60.5
HD069267	GS-2003B-Q-63	2003-11-27	0.5''	1 × 1	B600_G5323	508,512	60.5,60.5
HD145148	GS-2004A-Q-62	2004-04-21	0.5''	1 × 1	B600_G5323	508,512	60.5,60.5
HD165760	GS-2004A-Q-62	2004-07-20	0.5''	1 × 1	B600_G5323	508,512	120.5,120.5

NOTE. — For the GMOS-N observations setting A (2×2 binning and 0.75'' wide slits) we obtained observations for 6 stars with 13 individual exposures, while for setting B (1×1 binning and 0.5'' slit width) we observed 11 stars with 35 individual exposures. For the GMOS-S observations in setting B (1×1 binning and 0.5'' slit width) we observed 10 stars with 20 individual exposures.

Wavelength calibration was done by fitting 4th-order Chebyshev polynomials to the positions of lines identified in CuAr arc lamp spectra, taken close in time of the stellar observations. The rms of the wavelength solutions was typically 0.2 Å. The wavelength solutions were measured on the 2D spectra using the IRAF tasks AUTOIDENTIFY and REIDENTIFY and applied to the Lick standard star observations using the task TRANSFORM.

3.3. Scattered Light Subtraction

GMOS data suffer from scattered light, especially for central wavelengths shorter than 5200 Å. After the spectra were wavelength calibrated the IRAF task APSCATTER was used to fit the diffuse background light in each frame. Particular care was taken to fit and subtract the background light and not the light from the wings of the PSF. Fit orders of 11 in X and 7 in Y gave good results. This step significantly improved the results for several of the stars, especially those of earlier spectral types. We point out that since the scattered-light component is a smoothly varying function of detector position that changes on spatial scales much larger than the individual absorption features measured by a Lick index, the contribution to the total Lick index uncertainty as-

sociated with this subtraction is negligible compared to variations in the sky subtraction.

3.4. Quantum Efficiency Corrections

The three CCDs in each GMOS detector array were chosen to have similar quantum efficiency (QE) characteristics but there are still differences of a few percent that depend on wavelength. A method was developed to measure the relative QE curves of CCDs 1 and 3 relative to CCD 2. A correction to the QE differences as a function of wavelength can then be applied. This can further reduce or remove intensity jumps at the chip boundaries. This correction step is now being implemented in the Gemini GMOS IRAF package.

3.5. Parallactic Angle Slit-Loss Corrections

The GMOS instruments do not have atmospheric dispersion correctors (ADCs) so unless a slit is placed along the parallactic angle at the time of the observation there will be wavelength-dependent slit losses (Filippenko 1982). An IDL procedure was developed to calculate the slit losses based on the difference between the position angle (PA) of an observation and the parallactic angle and a correction applied to the spectra. While

this does not restore the lost flux it is important for making the continuum shapes from different observations similar enough that these spectra can be successfully averaged.

3.6. Flux Calibration

Relative flux calibrations were performed with observations of flux standard stars and analyzed with the IRAF tasks STANDARD and SENSFUNC (via the Gemini task GSSTANDARD). The GMOS-N data were calibrated using observations of EG131 taken in June 2002. The mean atmospheric extinction curve for Mauna Kea from the Gemini IRAF package was used. The GMOS-S data were calibrated using an observation of LTT 9239 from November 2003. The atmospheric extinction curve for Cerro Paranal obtained from the ESO web site was used for the GMOS-S data.

Each flux-calibrated spectrum was compared by eye with reference spectra of similar spectral type from the MILES library (Vazdekis et al. 2010) and duplicate observations of the same stars obtained with VLT/FORS (Puzia et al. 2005). We define the final sample of high-quality GMOS Lick standard-star spectra as those spectra for which we find flux discrepancies smaller than 20% between their final flux calibration and the reference spectra mentioned above. The final sample spectra can be downloaded from the GMOS calibration web page <http://www.gemini.edu/node/10697>.

3.7. Radial Velocity Measurements

To derive the rest-frame radial velocity of each Lick standard star we use the spectroscopic stellar library, STELIB⁵ which consists of a homogeneous set of stellar spectra with various spectral types, luminosity classes, and metallicities in the wavelength range 3200–9500 Å, with a spectral resolution of ~ 3 Å (see Le Borgne et al. 2003). The overall absolute photometric uncertainty of this library is 3% and it provides an excellent reference frame in terms of spectral type and spectral resolution, matching the properties of our GMOS spectra and allowing us to derive accurate radial velocity measurements while testing the influence of spectral mismatch.

We use the FXCOR package in the IRAF environment (Tody 1993) to derive radial velocities over the full wavelength coverage of our Lick standard spectra. We filter both object and template star spectra with a Welch filter⁶ and fit the cross-correlation function peak with a Gaussian. Recorded radial velocities are the corresponding values at the peak of the cross-correlation function.

Mismatch in spectral type between object and template spectrum translates in increased radial velocity errors and we determine the impact of this systematic uncertainty in the following analysis. For the full sample of Lick standard star spectra we compute the radial velocity mean and dispersion for each star using the entire STELIB library and reject clear outliers in radial velocity space using Chauvenet criteria⁷. The typical dispersion before the rejection of outliers is then 10–20 km/s which

⁵ Spectra are available at <http://webast.ast.obs-mip.fr/stelib>.

⁶ After extensive experimentation with the available Fourier filtering functions within FXCOR we converged on the Welch filter with the following parameters: CUTOFF=20, CUTOFF=1000, FULLON=30, and FULLOFF=800.

⁷ Based on the mean and standard deviation of n data points, a

TABLE 2
FITTING FUNCTIONS OF GMOS SPECTRAL RESOLUTION

setup	a	$b \cdot 10^{-3}$	$c \cdot 10^{-7}$	rms
GMOS-N/A	8.86 ± 0.68	-2.03 ± 0.27	1.95 ± 0.25	0.071
GMOS-N/B	5.17 ± 0.44	-1.08 ± 0.17	1.06 ± 0.16	0.053
GMOS-S/B	5.17 ± 0.75	-0.91 ± 0.30	0.82 ± 0.28	0.089

NOTE. — The fitting functions give the spectral resolution in FWHM as a function of wavelength, both in units of Å.

is mainly driven by the contribution of template star mismatch. The total error budget is $\sigma_{\text{total}}^2 = \sigma_{\text{stat.}}^2 + \sigma_{\text{templ.}}^2$ and is a linear combination of statistical and template mismatch error. Reducing the sample of template stars to only those within two spectral types of the Lick standard spectral type, we find that the dispersion decreases significantly below 10 km/s. The resulting error of the mean radial velocity is in all cases $\lesssim 1$ km/s. We conclude that selecting template stars with similar spectral types as the Lick standard stars is critical for radial velocity measurements with the cross-correlation technique and for a robust interpretation of the results at the instrumental resolutions probed by this study (see Sect. 2).

4. ANALYSIS

4.1. Spectral Resolution

The spectral resolution of our GMOS-N observations for the two instrument configurations was determined using the FWHM of wavelength-calibration lamp emission lines and found to be very well approximated by polynomial functions for the instrument setup A ($2 \times 2-0.75''$) and setup B ($1 \times 1-0.5''$):

$$\text{FWHM}_i(\lambda) = a + b\lambda + c\lambda^2$$

where $\text{FWHM}_i(\lambda)$ is for the i -th setup. λ is in units of Å. Table 2 summarizes the coefficients and quantifies the fit quality for all instrumental setups. Note that for instrument setup B the spectral resolutions of GMOS-N and GMOS-S are relatively similar and that all three GMOS configurations are significantly smaller than the nominal spectral resolution of the Lick index systems (Worthey & Ottaviani 1997). The spectral resolutions of the various GMOS configurations and the Lick/IDS resolution are shown in Figure 1. These analytic functions serve as baseline to broaden the GMOS spectra to the Lick/IDS spectral resolution before applying the index measuring routines. The smoothing of our sample spectra is performed with a wavelength-dependent Gaussian kernel with

$$\sigma_{\text{smooth}}(\lambda) = \left(\frac{\text{FWHM}(\lambda)_{\text{Lick}}^2 - \text{FWHM}(\lambda)_i^2}{8 \ln 2} \right)^{\frac{1}{2}}$$

where FWHM_i describes the spectral resolution of the corresponding instrument setup.

4.2. Lick Index Measurements

A crucial part of measuring the strength of spectroscopic absorption or emission features is the accurate definition of the adjacent continuum. The Lick system bypasses this complication by defining a *pseudo*-continuum

measurement can be discarded as an outlier if its normal distribution probability is less than $(2n)^{-1}$ (see e.g. Peirce 1852).

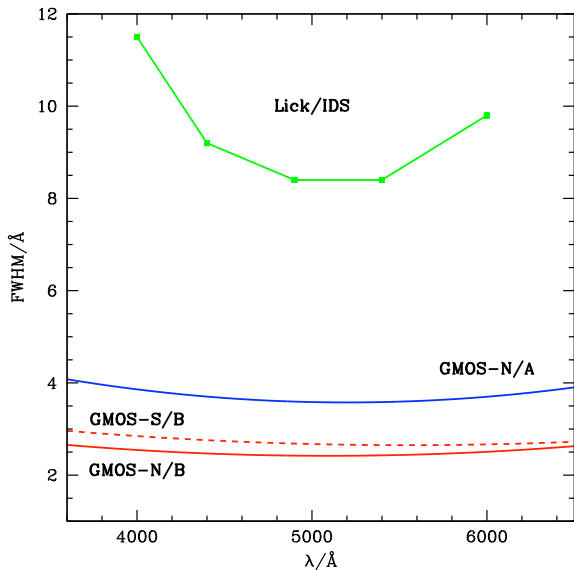


FIG. 1.— Comparison of the Lick/IDS spectral resolution which is implicitly hardwired in the Lick index system and the corresponding resolutions for our three GMOS instrument configurations.

around strong absorption features of interest, as illustrated in Figure 2. To determine the continuum level inside the feature passband a linear interpolation of the mean fluxes in two satellite passbands is performed which defines the *pseudo*-continuum flux F_c . The feature and *pseudo*-continuum passband definitions are summarized in Table A1.

The flux ratio in the feature passband between the absorption line F_l and the *pseudo*-continuum F_c is then used to define the line index

$$I_a = \int_{\lambda_{\min}}^{\lambda_{\max}} \left(1 - \frac{F_l(\lambda)}{F_c(\lambda)} \right) d\lambda \quad (1)$$

in units of \AA , where λ_{\min} and λ_{\max} define the blue and red boundaries of the feature passband, respectively (see Figure 2). Note that if F_c were the *true* continuum, I_a would closely resemble an equivalent width. The subscript “a” indicates that the line index definition in Equation 1 is used for narrow atomic absorption features which are calculated in \AA ngström. For molecular absorption features the line index is defined as

$$I_m = -2.5 \log \left[\frac{1}{\Delta\lambda} \int_{\lambda_{\min}}^{\lambda_{\max}} \frac{F_l(\lambda)}{F_c(\lambda)} d\lambda \right] \quad (2)$$

in units of magnitudes⁸, where $\Delta\lambda = \lambda_{\max} - \lambda_{\min}$. The transformation between the \AA ngström and magnitude scale can be performed with the following two equations

$$I_a = \Delta\lambda (1 - 10^{-0.4 I_m}) \quad (3)$$

$$I_m = -2.5 \log \left(1 - \frac{I_a}{\Delta\lambda} \right) \quad (4)$$

The Lick line index strengths for our sample stars, as defined by Equations 1 and 2 together with the passband definitions summarized in Table A1, were measured

⁸ One exception is the G4300 index which is traditionally measured in \AA , although the strength of the dominant feature is driven by the CH molecule abundance.

with the GONZO code that is described in detail in Puzia et al. (2002, 2005). The GMOS science and variance spectra are used to generate the uncertainty of the Lick index measurements via Monte Carlo simulations. The indices are re-measured on the Poisson noise-altered spectra. From the distribution of index values the $1\text{-}\sigma$ standard deviation defines the total Lick index uncertainty. Note that instead of transforming the spectrum to the restframe the code shifts the index passbands to the observed redshift to avoid pixel noise correlation effects for narrowly defined indices.

4.3. Lick Index-System Calibration

Using the full dataset we determine the mean index correction terms to the Lick system for each instrument setup and calculate the corresponding r.m.s. For each index, outliers are rejected using Chauvenet criteria as described above. From the selected data we derive the mean correction in the sense

$$I_{\text{Lick}} = I_{\text{GMOS}} + \delta \quad (5)$$

(see dashed lines in Figures 3, 4 and 5), the error of the mean correction, $\Delta\delta$, and the dispersion, $\sigma(\delta)$. The numerical values of these parameters are summarized in columns two to four of Tables A2, A3 and A4. We also fit linear relations of the form

$$I_{\text{Lick}} = a \times I_{\text{GMOS}} + b \quad (6)$$

to the selected data (dotted lines in Figures 3, 4 and 5) and determine the uncertainties, Δa and Δb , as well as the root mean square and the range over which the fit is valid. All parameter values are tabulated in columns five to eleven of Tables A2, A3, and A4. Note that our Lick standard-star sample covers a large dynamic range in each index allowing for a robust correction as a function of index strength. Figures 3, 4 and 5 illustrate the comparison between Lick index system and our measurements for the three instrument configurations. The plots show the overall quality of the Lick index calibration for the three spectroscopic settings. We point out that although the sampling range of each index varies from epoch to epoch the overall fit quality is not driven by any particular sub-sample. In particular, the most important Lick indices that are typically used in stellar population analyses (marked by bold panels in Figures 3, 4 and 5) show very consistent calibrations.

The previous Lick index calibrations are strictly valid only for stellar systems with zero line of sight velocity dispersion (LOSVD). If objects such as massive galaxies are observed with complex LOSVD distribution functions, higher-order correction terms for the LOSVD broadening of the indices is required. Such correction terms are provided in Kuntschner (2004). However, for stellar systems with low LOSVD (i.e. $\sigma < 50$ km/s) such as globular clusters and dwarf galaxies these corrections are less than 1% and can be safely neglected.

5. SUMMARY

We provide Lick index calibration functions for the GMOS-N and GMOS-S spectrograph using two instrumental configurations, namely with 2×2 binning and $0.75''$ slit width (setup A) and with 1×1 binning and $0.5''$ slit width (setup B). The quality of the linear correction terms shows that widely-used Lick indices such as

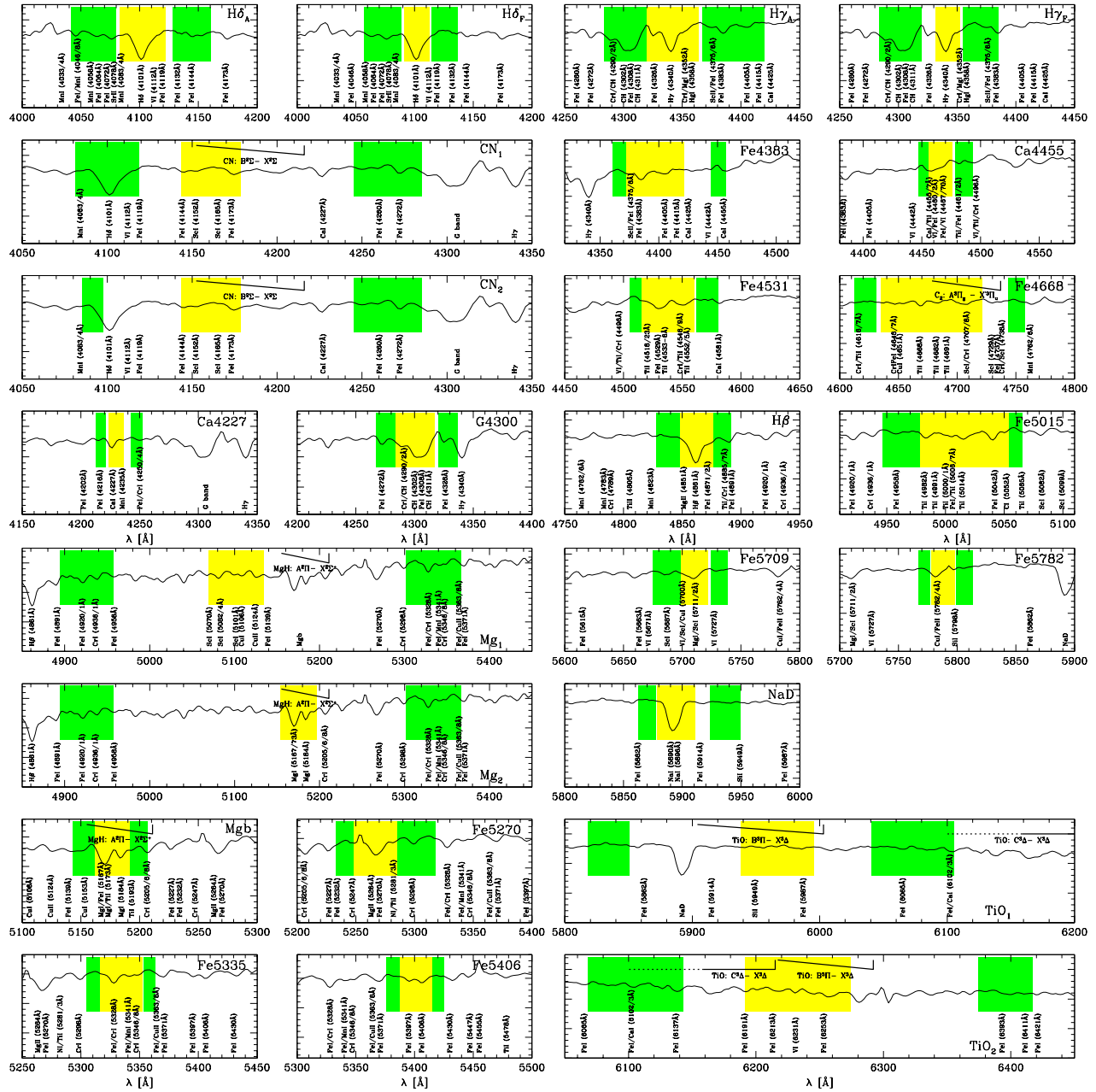


FIG. 2.— Illustration of Lick index passband definitions for the 25 indices as defined in Table A1. Green and yellow shaded regions mark the continuum and feature passbands, respectively. Satellite absorption lines as well as molecular bands are indicated (Reader & Corliss 1981; Pearse & Gaydon 1976) together with the spectrum of the Milky Way globular cluster NGC 6284, taken from Puzia et al. (2002).

the Balmer indices $H\beta$, $H\gamma_A$, and $H\delta_A$ along with metallicity sensitive indices Fe5015, Fe5270, Fe5335, Fe5406, Mg_2 and Mgb can be robustly calibrated and thus used to derive stellar population parameters by comparison with predictions of stellar population synthesis models that use the exact same Lick index definitions. Indices which sample many weak features or molecular absorption bands, such as Mg_1 , TiO_1 and TiO_2 , with very wide wavelength coverage or indices with particularly narrow passband definitions, such as Fe4384, Ca4455, Fe4531, Ca4227, and Fe5782, are less robustly calibrated and should be used with caution.

We gratefully acknowledge the thoughtful comments and suggestions of the anonymous referee. T.H.P. acknowledges support by CONICYT through FONDE-

CYT/Regular Project No. 1121005, FONDAF Center for Astrophysics (15010003) and BASAL Center for Astrophysics and Associated Technologies (PFB-06), Conicyt, Chile. Based on observations obtained at the Gemini Observatory, which is operated by the Association of Universities for Research in Astronomy, Inc., under a cooperative agreement with the NSF on behalf of the Gemini partnership: the National Science Foundation (United States), the Science and Technology Facilities Council (United Kingdom), the National Research Council (Canada), CONICYT (Chile), the Australian Research Council (Australia), Ministério da Ciência, Tecnologia e Inovação (Brazil) and Ministerio de Ciencia, Tecnología e Innovación Productiva (Argentina).

Facilities: Gemini (GMOS).

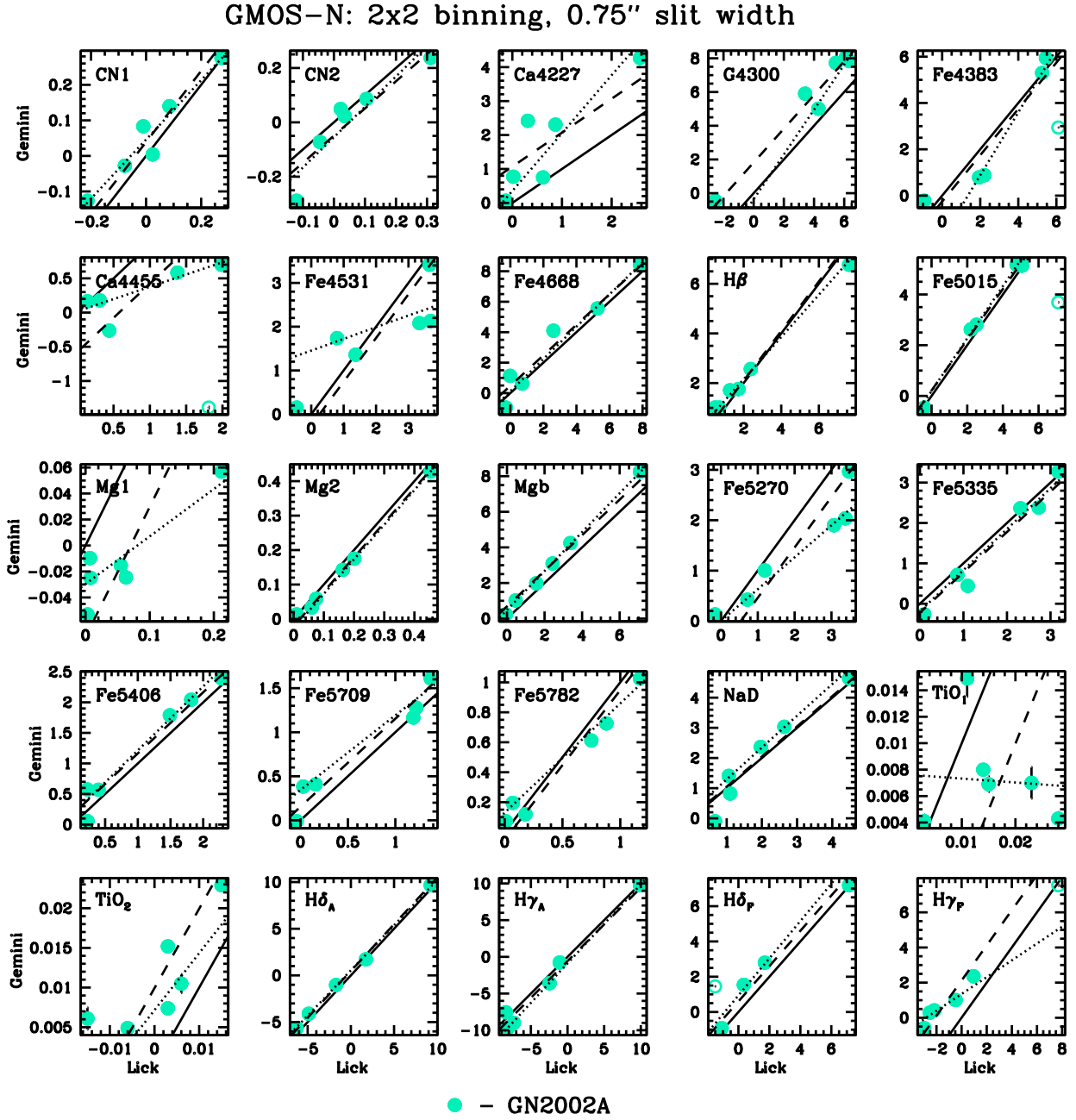


FIG. 3.— Comparison plots between original Lick system measurements and Lick index measurements from our standard-star GMOS-N spectra obtained with setup A: 2×2 binning and $0.75''$ slit width. In each panel, the solid lines are the identity relations, while dashed lines illustrate the mean linear offset corrections. Dotted lines are weighted least-square fits to the solid data points. Open circles mark data that were rejected using Chauvenet criteria (see text for details). The corresponding correction terms are summarized in Table A2. Note that very few data points have error bars larger than the symbol size.

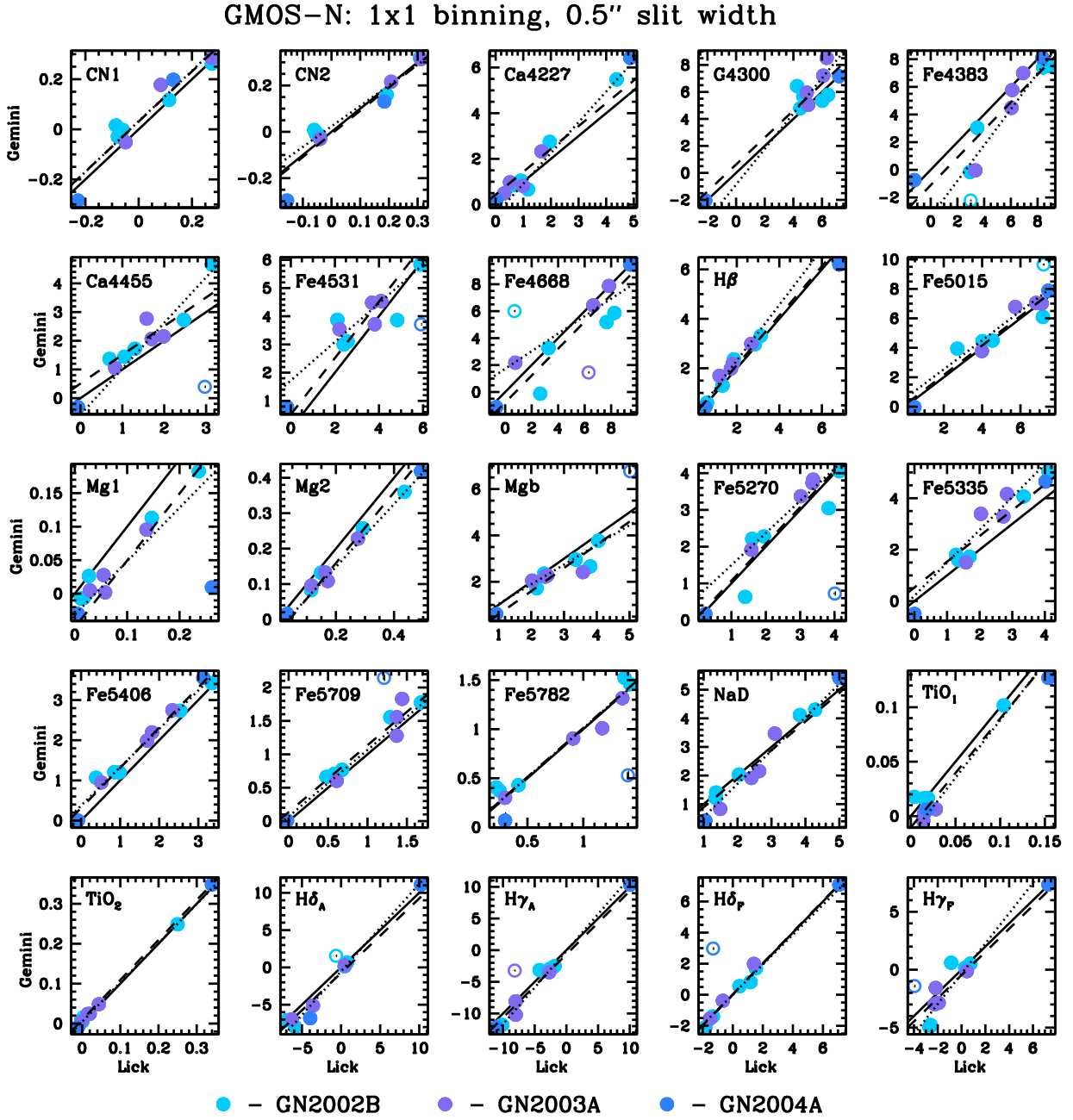


FIG. 4.— Comparison plots similar to Figure 3, but this time for GMOS-N spectra obtained with setup B: 1×1 binning and $0.5''$ slit width. The different color shadings indicate three different data set from the observing periods 2002B, 2003A, and 2004A. The corresponding correction terms are summarized in Table A3.

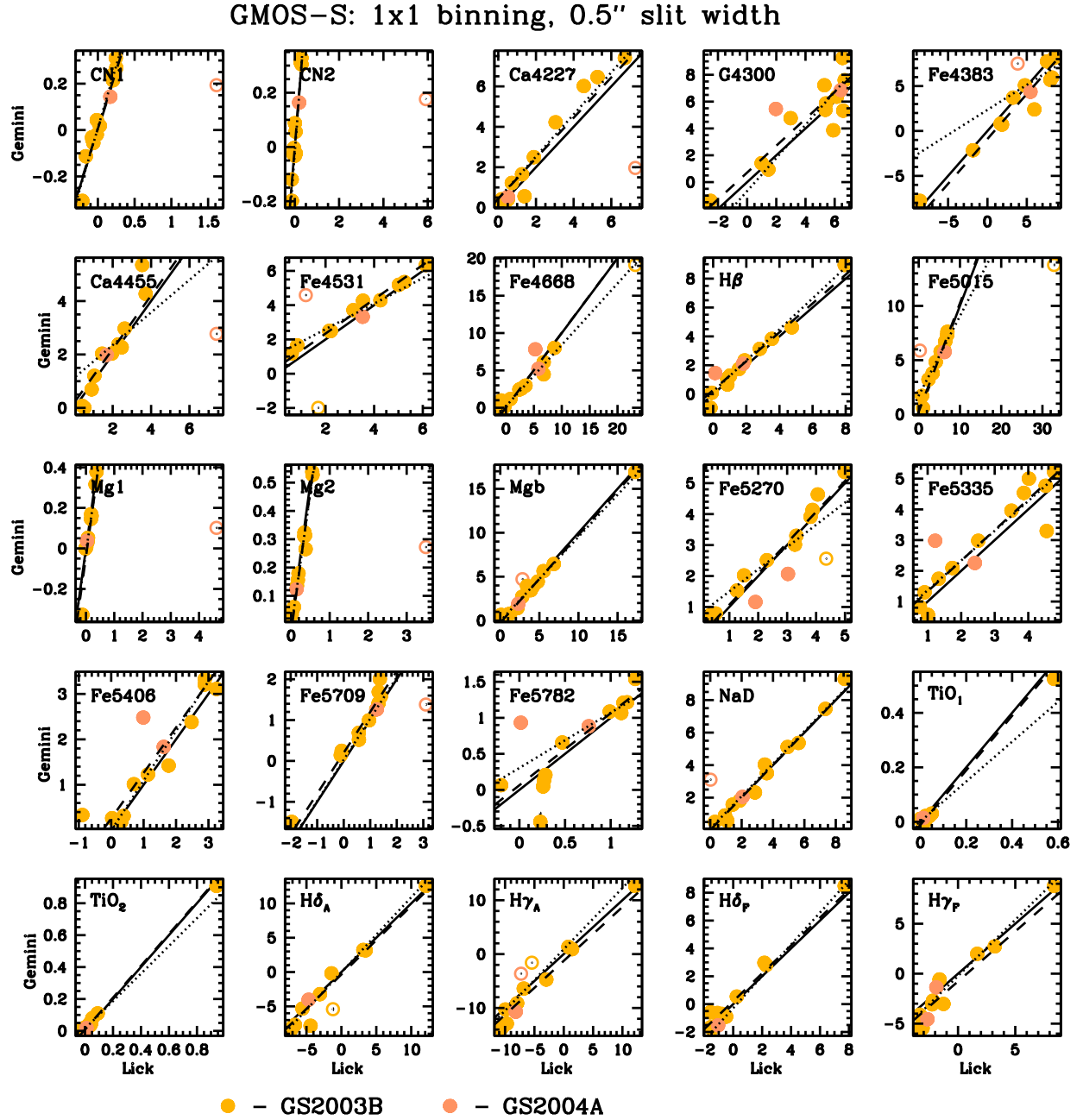


FIG. 5.— Comparison plots similar to Figure 3, but this time for GMOS-S spectra obtained with setup B: 1×1 binning and $0.5''$ slit width. The different color shadings indicate two different data set from the observing periods 2003B, and 2004A. The corresponding correction terms are summarized in Table A4.

REFERENCES

- Burstein, D., Faber, S. M., Gaskell, C. M., & Krumm, N. 1984, *ApJ*, 287, 586
- Faber, S. M., Friel, E. D., Burstein, D., & Gaskell, C. M. 1985, *ApJS*, 57, 711
- Filippenko, A. V. 1982, *PASP*, 94, 715
- Kotulla, R., Fritze, U., Weilbacher, P., & Anders, P. 2009, *MNRAS*, 396, 462
- Kroupa, P. 2001, *MNRAS*, 322, 231
- Kuntschner, H. 2004, *A&A*, 426, 737
- Kuntschner, H., Emsellem, E., Bacon, R., et al. 2006, *MNRAS*, 369, 497
- Le Borgne, J.-F., et al. 2003, *A&A*, 402, 433
- Nesterov, V. V., Kuzmin, A. V., Ashimbaeva, N. T., et al. 1995, *A&AS*, 110, 367
- Pearse, R. W. B. & Gaydon, A. G. 1976, *The Identification of Molecular Spectra*, Fourth Edition, Chapman and Hall, London
- Peirce, B. 1852, *AJ*, 2, 161
- Puzia, T. H., Saglia, R. P., Kissler-Patig, M., Maraston, C., Greggio, L., Renzini, A., & Ortolani, S. 2002, *A&A*, 395, 45
- Puzia, T. H., Kissler-Patig, M., Thomas, D., Maraston, C., Saglia, R. P., Bender, R., Goudfrooij, P., & Hempel, M. 2005, *A&A*, 439, 997
- Reader J. & Corliss Ch.H. 1981, *CRC Handbook of Chemistry and Physics*
- Thomas, D., Maraston, C., & Bender, R. 2003, *MNRAS*, 339, 897
- Thomas, D., Maraston, C., & Korn, A. 2004, *MNRAS*, 351, L19
- Thomas, D., Maraston, C., Bender, R., & Mendes de Oliveira, C. 2005, *ApJ*, 621, 673
- Tody, D. 1993, *Astronomical Data Analysis Software and Systems II*, 52, 173
- Trager, S. C., Worthey, G., Faber, S. M., Burstein, D., & Gonzalez, J. J. 1998, *ApJS*, 116, 1
- Trager, S. C., Faber, S. M., Worthey, G., & González, J. J. 2000, *AJ*, 119, 1645
- Tripicco, M. J., & Bell, R. A. 1995, *AJ*, 110, 3035
- Vazdekis, A. 1999, *ApJ*, 513, 224
- Vazdekis, A., Sánchez-Blázquez, P., Falcón-Barroso, J., Cenarro, A. J., Beasley, M. A., Cardiel, N., Gorgas, J., & Peletier, R. F. 2010, *MNRAS*, 404, 1639
- Worthey, G. 1994, *ApJS*, 95, 107
- Worthey, G., Faber, S. M., Gonzalez, J. J., & Burstein, D. 1994, *ApJS*, 94, 687
- Worthey, G., & Ottaviani, D. L. 1997, *ApJS*, 111, 377

TABLE A1
LICK INDEX PASSBAND DEFINITIONS

Index	feature passband		blue continuum		red continuum		units
H δ_A	4083.500	4122.250	4041.600	4079.750	4128.500	4161.000	Å
H δ_F	4091.000	4112.250	4057.250	4088.500	4114.750	4137.250	Å
CN ₁	4143.375	4178.375	4081.375	4118.875	4245.375	4285.375	mag
CN ₂	4143.375	4178.375	4085.125	4097.625	4245.375	4285.375	mag
Ca4227	4223.500	4236.000	4212.250	4221.000	4242.250	4252.250	Å
G4300	4282.625	4317.625	4267.625	4283.875	4320.125	4336.375	Å
H γ_A	4319.750	4363.500	4283.500	4319.750	4367.250	4419.750	Å
H γ_F	4331.250	4352.250	4283.500	4319.750	4354.750	4384.750	Å
Fe4383	4370.375	4421.625	4360.375	4371.625	4444.125	4456.625	Å
Ca4455	4453.375	4475.875	4447.125	4455.875	4478.375	4493.375	Å
Fe4531	4515.500	4560.500	4505.500	4515.500	4561.750	4580.500	Å
Fe4668	4635.250	4721.500	4612.750	4631.500	4744.000	4757.750	Å
H β	4847.875	4876.625	4827.875	4847.875	4876.625	4891.625	Å
Fe5015	4977.750	5054.000	4946.500	4977.750	5054.000	5065.250	Å
Mg ₁	5069.125	5134.125	4895.125	4957.625	5301.125	5366.125	mag
Mg ₂	5154.125	5196.625	4895.125	4957.625	5301.125	5366.125	mag
Mgb	5160.125	5192.625	5142.625	5161.375	5191.375	5206.375	Å
Fe5270	5245.650	5285.650	5233.150	5248.150	5285.650	5318.150	Å
Fe5335	5312.125	5352.125	5304.625	5315.875	5353.375	5363.375	Å
Fe5406	5387.500	5415.000	5376.250	5387.500	5415.000	5425.000	Å
Fe5709	5698.375	5722.125	5674.625	5698.375	5724.625	5738.375	Å
Fe5782	5778.375	5798.375	5767.125	5777.125	5799.625	5813.375	Å
NaD	5878.625	5911.125	5862.375	5877.375	5923.875	5949.875	Å
TiO ₁	5938.375	5995.875	5818.375	5850.875	6040.375	6105.375	mag
TiO ₂	6191.375	6273.875	6068.375	6143.375	6374.375	6416.875	mag

NOTE. — The above passband definitions are for the full set of 25 Lick indices which are used in this work. The index definitions were taken from Worthey (1994) and Worthey & Ottaviani (1997). The units of each index are given in the last column.

APPENDIX
APPENDIX MATERIAL

TABLE A2
LICK INDEX CORRECTION TERMS FOR GMOS-N WITH 2×2 BINNING AND $0.75''$ SLITWIDTH

Index	δ	$\Delta\delta$	$\sigma(\delta)$	a	Δa	b	Δb	r.m.s.	min	max
H δ_A	-0.50	0.14	0.31	0.9679	0.0325	0.5751	0.1159	0.1446	-6.28	9.25
H δ_F	-0.62	0.27	0.60	1.0557	0.2375	0.9616	0.2977	0.4061	-1.08	7.15
CN ₁	-0.04	0.02	0.05	0.8327	0.1112	0.0468	0.0166	0.0331	-0.21	0.27
CN ₂	0.05	0.03	0.07	1.1163	0.2299	-0.0559	0.0355	0.0643	-0.12	0.31
Ca4227	-1.06	0.33	0.82	1.7038	0.2406	0.3610	0.1383	0.2745	-0.13	2.57
G4300	-1.84	0.26	0.64	1.3301	0.3060	-0.3287	1.5129	0.5887	-2.56	6.33
H γ_A	0.55	0.43	1.05	1.0773	0.0765	-0.8482	0.3727	0.4720	-8.41	9.88
H γ_F	-2.14	0.27	0.65	0.4789	0.1119	1.3354	0.1561	0.1950	-2.97	0.95
Fe4383	0.24	0.39	0.95	1.3613	0.0986	-1.8227	0.3556	0.2811	-0.94	5.45
Ca4455	0.58	0.22	0.53	0.3581	0.1586	0.0142	0.1275	0.1498	0.14	1.99
Fe4531	0.25	0.40	0.99	0.2659	0.1394	1.4475	0.2532	0.3116	-0.45	3.69
Fe4668	-0.46	0.33	0.80	1.0582	0.1048	0.1047	0.3123	0.4892	-0.27	7.84
H β	-0.11	0.20	0.50	0.8531	0.0552	0.4547	0.0744	0.0921	0.48	7.61
Fe5015	-0.23	0.09	0.21	1.0324	0.0421	0.2096	0.1257	0.0696	-0.41	5.08
Mg ₁	0.07	0.02	0.05	0.3658	0.1210	-0.0299	0.0039	0.0071	0.00	0.21
Mg ₂	0.02	0.00	0.01	1.0037	0.0279	-0.0261	0.0027	0.0033	0.01	0.45
Mgb	-0.67	0.13	0.32	1.0912	0.0244	0.5020	0.0439	0.0648	-0.06	7.08
Fe5270	0.53	0.25	0.62	0.6325	0.0589	-0.0035	0.1085	0.1346	-0.16	3.48
Fe5335	0.23	0.12	0.29	1.0152	0.1011	-0.1927	0.1602	0.1621	0.10	3.18
Fe5406	-0.16	0.08	0.19	1.0458	0.0577	0.1624	0.0574	0.0712	0.23	2.28
Fe5709	-0.15	0.06	0.15	0.8457	0.0665	0.3407	0.0473	0.0767	-0.04	1.37
Fe5782	0.05	0.05	0.12	0.7298	0.0504	0.1282	0.0284	0.0439	0.01	1.17
NaD	-0.04	0.19	0.47	1.0533	0.1386	0.2238	0.2307	0.2060	0.67	4.48
TiO ₁	0.01	0.00	0.01	-0.0298	0.1490	0.0076	0.0023	0.0018	0.00	0.03
TiO ₂	-0.01	0.00	0.01	0.7194	0.3193	0.0072	0.0018	0.0031	-0.02	0.02

NOTE. — See Figure 3 for an illustration of the corresponding Lick index corrections that are being used in Equations 5 and 6.

TABLE A3
LICK INDEX CORRECTION TERMS FOR GMOS-N WITH 1×1 BINNING AND $0.5''$ SLITWIDTH

Index	δ	$\Delta\delta$	$\sigma(\delta)$	a	Δa	b	Δb	r.m.s.	min	max
H δ_A	0.79	0.37	1.17	1.1717	0.0757	-0.4964	0.2786	0.5903	-6.90	10.23
H δ_F	-0.05	0.09	0.28	0.9631	0.0950	-0.0115	0.1211	0.3197	-1.83	7.09
CN ₁	-0.03	0.02	0.05	1.0086	0.1085	0.0311	0.0175	0.0480	-0.23	0.28
CN ₂	0.01	0.02	0.06	0.8878	0.0799	0.0227	0.0145	0.0344	-0.16	0.31
Ca4227	-0.42	0.17	0.58	1.3450	0.1078	-0.4221	0.1431	0.2317	0.02	4.87
G4300	-0.60	0.30	0.99	1.3118	0.4031	-0.8420	2.3819	0.6974	-2.15	7.21
H γ_A	0.71	0.30	0.99	1.1590	0.0861	-0.0725	0.6055	0.7477	-11.07	10.07
H γ_F	0.49	0.35	1.15	1.3066	0.1587	-0.3130	0.2959	0.5955	-2.69	7.30
Fe4383	1.09	0.39	1.30	1.2981	0.1648	-3.3554	1.0112	0.6174	-1.22	8.82
Ca4455	-0.50	0.16	0.52	1.5966	0.1529	-0.5676	0.2829	0.2143	-0.06	3.14
Fe4531	-0.53	0.23	0.77	0.6841	0.0868	1.7106	0.3664	0.2408	-0.17	5.89
Fe4668	0.76	0.43	1.43	0.6495	0.1602	1.7043	1.0444	0.7967	-0.68	9.44
H β	-0.14	0.10	0.32	1.1268	0.0717	0.0715	0.1299	0.1292	0.52	6.82
Fe5015	-0.14	0.21	0.69	0.9854	0.1688	0.5641	0.9325	0.5689	0.47	7.46
Mg ₁	0.05	0.02	0.07	0.7968	0.1320	-0.0307	0.0122	0.0229	0.01	0.26
Mg ₂	0.04	0.01	0.02	0.8887	0.0651	-0.0282	0.0136	0.0164	0.03	0.49
Mgb	0.42	0.12	0.41	0.8506	0.1208	0.1787	0.3965	0.2749	0.93	4.05
Fe5270	-0.08	0.15	0.50	0.8737	0.1124	0.6210	0.3245	0.2457	0.24	4.14
Fe5335	-0.52	0.17	0.57	1.2776	0.2528	0.2193	0.5998	0.5570	0.00	4.11
Fe5406	-0.32	0.05	0.18	0.9559	0.0417	0.3658	0.0758	0.0912	-0.08	3.35
Fe5709	-0.13	0.04	0.14	0.9953	0.1638	0.0651	0.1981	0.1644	-0.02	1.68
Fe5782	-0.01	0.04	0.13	0.9982	0.0549	0.0087	0.0512	0.0578	0.22	1.42
NaD	0.12	0.12	0.39	1.1631	0.1124	-0.6259	0.2883	0.2969	1.05	5.00
TiO ₁	0.01	0.00	0.01	1.0604	0.1106	-0.0175	0.0029	0.0052	0.00	0.15
TiO ₂	-0.01	0.00	0.00	0.9829	0.0103	0.0051	0.0005	0.0012	-0.01	0.34

NOTE. — See Figure 4 for an illustration of the corresponding Lick index correction terms that are being used in Equations 5 and 6.

TABLE A4
 LICK INDEX CORRECTION TERMS FOR GMOS-S WITH 1×1 BINNING AND $0.5''$ SLITWIDTH

Index	δ	$\Delta\delta$	$\sigma(\delta)$	a	Δa	b	Δb	r.m.s.	min	max
H δ_A	0.40	0.36	1.25	1.0919	0.1355	-0.0086	0.5216	0.8713	-7.11	12.11
H δ_F	-0.19	0.15	0.52	1.1447	0.0600	-0.2633	0.0711	0.2086	-1.57	7.71
CN ₁	-0.01	0.01	0.04	1.0735	0.0797	0.0121	0.0129	0.0413	-0.21	0.25
CN ₂	-0.01	0.01	0.05	1.0736	0.0920	-0.0058	0.0165	0.0459	-0.14	0.30
Ca4227	-0.46	0.18	0.64	1.0411	0.0201	0.4598	0.0447	0.1135	0.15	6.72
G4300	-0.69	0.40	1.48	1.2312	0.0832	-0.6426	0.5499	0.2172	-2.51	6.69
H γ_A	1.31	0.42	1.53	1.1368	0.1181	0.9595	0.8582	0.9515	-10.67	12.20
H γ_F	0.80	0.32	1.15	1.1245	0.0982	-0.2542	0.2450	0.4774	-3.33	8.39
Fe4383	0.85	0.36	1.31	0.5556	0.2616	2.3222	1.2843	0.4873	-8.58	8.47
Ca4455	-0.22	0.17	0.61	0.6107	0.2103	1.1178	0.3183	0.1305	0.42	3.72
Fe4531	-0.33	0.09	0.31	0.7437	0.1947	1.1023	0.6749	0.3376	0.61	6.13
Fe4668	-0.09	0.35	1.27	0.8227	0.0871	0.2525	0.3734	0.4080	-0.88	8.72
H β	-0.26	0.13	0.50	1.0757	0.0511	0.1672	0.0719	0.1347	-0.16	7.94
Fe5015	-0.32	0.14	0.50	0.7301	0.0845	1.7871	0.3799	0.2113	0.82	6.97
Mg ₁	0.03	0.01	0.05	0.9470	0.0279	-0.0077	0.0050	0.0115	-0.13	0.37
Mg ₂	0.02	0.01	0.03	0.9592	0.0123	-0.0091	0.0040	0.0073	0.02	0.56
Mg b	0.21	0.10	0.39	0.9570	0.0505	-0.0258	0.1613	0.1803	0.11	17.27
Fe5270	-0.08	0.13	0.47	0.7173	0.2012	0.7790	0.4942	0.3252	0.35	4.99
Fe5335	-0.32	0.18	0.68	0.9677	0.0881	0.3939	0.1904	0.2338	0.77	4.77
Fe5406	-0.27	0.15	0.53	1.0934	0.1120	0.0038	0.1577	0.1885	-0.89	3.25
Fe5709	-0.21	0.06	0.21	1.0091	0.1178	0.0406	0.1195	0.0674	-1.96	1.40
Fe5782	-0.06	0.10	0.36	0.7652	0.1222	0.3007	0.0719	0.0897	-0.20	1.27
NaD	-0.03	0.10	0.36	0.9969	0.0272	0.1169	0.0669	0.1350	0.30	8.57
TiO ₁	0.01	0.01	0.02	0.7323	0.1210	-0.0001	0.0029	0.0061	-0.00	0.58
TiO ₂	-0.01	0.01	0.02	0.8658	0.0952	0.0129	0.0034	0.0093	-0.02	0.94

NOTE. — See Figure 5 for an illustration of the corresponding Lick index correction terms that are being used in Equations 5 and 6.